

Chemical changes in groundwater due to flooding of an iron mine in a non-acid producing environment

Pauline Collon, Robert Fabriol, Michel Bues

► **To cite this version:**

Pauline Collon, Robert Fabriol, Michel Bues. Chemical changes in groundwater due to flooding of an iron mine in a non-acid producing environment. Ciccu R. 7th International Symposium on Environmental Issues and Waste Management in Energy and Mineral Production (SWEMP), Oct 2002, Cagliari, Italy. pp.761-768, 2002, Proceedings of the 7th International Symposium on Environmental Issues and Waste Management in Energy and Mineral Production (SWEMP). <hal-01343153>

HAL Id: hal-01343153

<https://hal.univ-lorraine.fr/hal-01343153>

Submitted on 12 Jul 2016

HAL is a multi-disciplinary open access archive for the deposit and dissemination of scientific research documents, whether they are published or not. The documents may come from teaching and research institutions in France or abroad, or from public or private research centers.

L'archive ouverte pluridisciplinaire **HAL**, est destinée au dépôt et à la diffusion de documents scientifiques de niveau recherche, publiés ou non, émanant des établissements d'enseignement et de recherche français ou étrangers, des laboratoires publics ou privés.

CHEMICAL CHANGES IN GROUNDWATER DUE TO FLOODING OF AN IRON MINE IN A NON-ACID-PRODUCING ENVIRONMENT

Pauline COLLON¹, Robert FABRIOL² and Michel BUES¹

¹ Laboratoire Environnement Géomécanique et Ouvrages
Ecole Nationale Supérieure de Géologie – Institut National Polytechnique de Lorraine
Rue du Doyen Marcel Roubault – BP 40 – 54501 Vandoeuvre-lès-Nancy Cedex – FRANCE

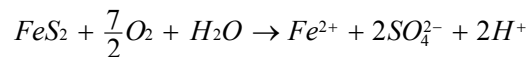
² BRGM
1av. du parc de Brabois - 54500 Vandoeuvre-lès-Nancy Cedex – FRANCE

INTRODUCTION

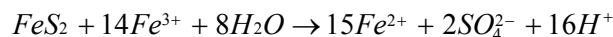
Mine drainage is one of the mining industry's undesirable effects on the environment. Mining operations disturb the chemical equilibrium of the surrounding rocks by suddenly exposing them to oxidising conditions. The chemical reactions that take place generate effluents that are usually acidic and contain SO_4^{2-} , Fe, Mn, etc. After the mines are closed and abandoned, the suspension of dewatering and drainage leads to progressive flooding of the workings. The waters drain these effluents to overflow points, springs and rivers. It is therefore necessary to predict any flow modifications and changes in water quality in order to install new management schemes for this resource.

MINE DRAINAGE IN LORRAINE

The oxidation of pyrite (FeS_2), the main cause of acid mine drainage (Rose and Cravotta, 2001; Razowska, 2001), occurs as soon as water, atmospheric oxygen and pyrite come into contact. When oxygen is the oxidising agent, the reaction is written:

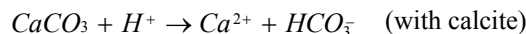


Pyrite can also be oxidised by ferric iron by the reaction (Smith and Svanks, 1970):



This reaction is very fast, especially at $\text{pH} < 4.5$. The reactivity of the system is sharply limited for Fe(III)/Fe(II) values below 0.2 and depends on a rapid Fe^{3+} input, usually supplied by bacterial catalysis of *Thiobacillus ferrooxidans* (Younger *et al.*, 1998).

If the environment is rich in carbonates, the acidity produced by pyrite oxidation is neutralised by the dissolution of the carbonates (Younger *et al.*, 1998; Salomons, 1995):



This is referred to as Neutral Mine Drainage (NMD). The reaction produces large amounts of Ca^{2+} ions which, given the high activity of SO_4^{2-} , can precipitate in the form of gypsum ($\text{CaSO}_4 \cdot 2\text{H}_2\text{O}$). Although the presence of gypsum in such environments has not yet been reported, a number of geochemical modelling studies have identified this reaction (Brown and Lawson, 1997; Donovan *et al.*, 2000; Mayo *et al.*, 2000). NMD effluents have a pH ranging from 6 to 8 and generally display high concentrations of SO_4 (up to 2900 mg/l), Ca (up to 660 mg/l) and HCO_3 (100-300 mg/l) (Smith and Brady, 2001). The quantities of Fe and Mn may also be high, over 2 and 5 mg/l respectively. NMD is chiefly known and investigated in connection with coal mines.

The Lorraine iron-bearing deposit, dating from the Late Lias, is formed of alternating marly levels (intercalations) and ferruginous limestone (mineralised layers) corresponding to a regressive sequence (Bubenicek, 1970). Moving upwards, transition from the marly facies into the lowest mineralised facies is progressive via a metre-scale intermediate or 'basal' layer. On top of the mineralised facies, i.e. in the hanging wall, transition into the next overlying marl intercalation occurs via a coarse-grained shelly limestone level known locally as 'crassin'. The iron-bearing formation can therefore be considered as a succession of elementary 'marl' - ore units (Figure 1) and displays very high carbonate contents (20 to 50% by weight of calcite). The whole succession is overlain by Bajocian micaceous marls. Mining has caused the fracturing and partial destruction of this impermeable level, enabling water from the Dogger limestone aquifer to infiltrate into the mine galleries.

These specific hydrogeological conditions make the Lorraine formation an original case of NMD. Since the northern sector of the Briey Basin is to be flooded in late 2002, this work aims to: (i) refine the understanding of mineralisation mechanisms of the water during and after flooding; and (ii) provide basic data for a hydrochemical simulator to construct a water-management model.

REACTIVITY OF MATERIALS IN THE LORRAINE IRON BASIN: EXPERIMENTAL STUDY

Our experimental studies were focused on 'marls' which, according to the results of Hervé (1980), release the largest quantity of sulphates. Thirteen samples were collected in the mine concessions still being drained in the northern part of the Briey basin, where three mineralised layers are accessible (Figure 1), namely, from deepest to shallowest, the brown, grey (containing "crassin") and yellow layers. Like the grey layer, the yellow layer is separated from the overlying marly intercalation by "crassin" of variable thickness (0 to 50 cm).

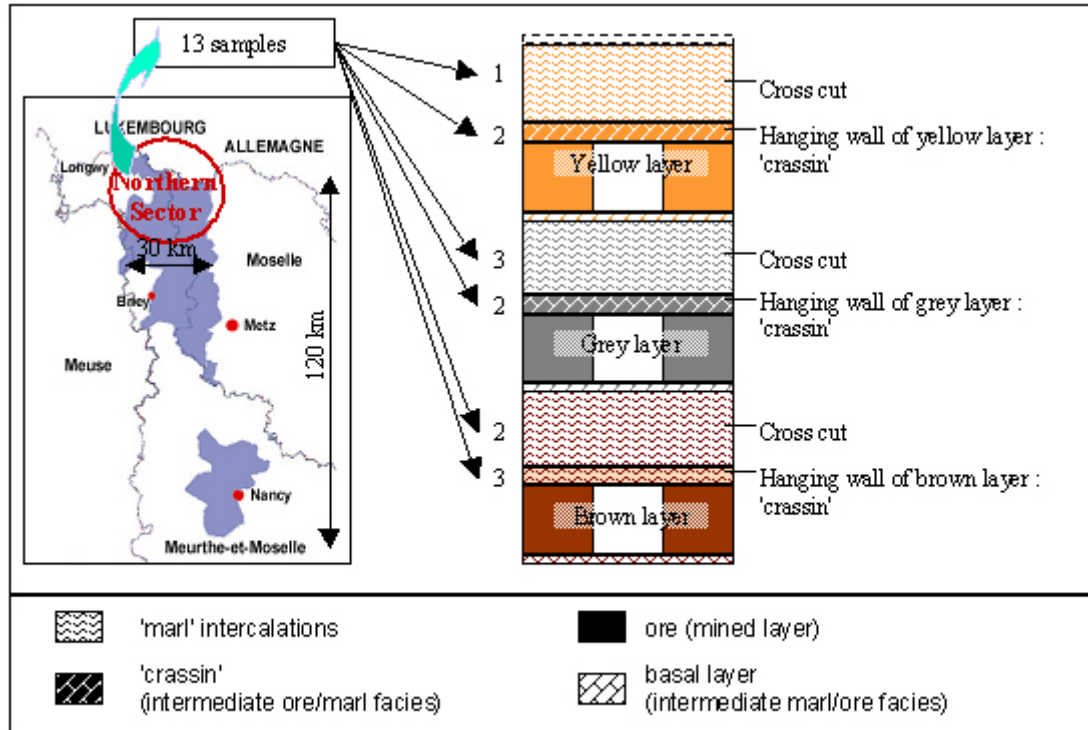
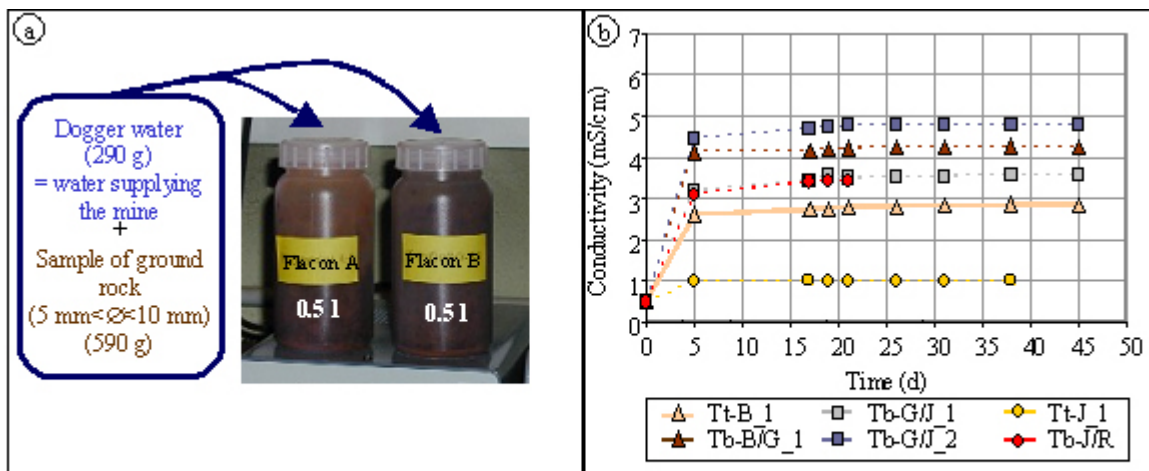


Figure 1 : Geographical and lithological distribution of the studied samples

Samples of about 30-40 kg were taken directly in the hanging walls of the layers or in the cross-cuts. Six samples were ground by a jaw crusher and sieved (cutoffs at 50 mm, 40 mm, 21.5 mm, 20 mm, 10 mm and 5 mm).

Closed reactor tests

The aim of the closed reactor tests was to characterise the chemical equilibrium. In 0.5-litre inert polypropylene bottles, 590 g of rock (5 mm$\leq\phi\leq 10\text{ mm}$) was brought into contact with 290 g of Dogger water. Each test was duplicated (bottles A and B, Figure 2a).



Designation of samples: i) Tt: top (hanging wall) or Tb: cross-cut ('marls'). ii) Lithology: B (brown), G (grey), J (yellow), R (red). 'f' meaning 'between the layers' and iii) sample No. (up to 3 in the same layer).

Figure 2 : Principle of closed reactor tests (a) and conductivity monitoring (b).

The conductivity was regularly measured in bottle B, until its value stabilised after about 36 days (Figure 2b). At this stage, water-rock chemical equilibrium is assumed and a sample was taken from bottle A, which had remained closed throughout the experiment. Conductivity and pH were measured in both bottles and yielded identical results, indicating

the repetitivity of the test.

Examination of the conductivity measurements reveals different chemical behaviours due to lateral and vertical variations in mineralogical composition. At the rock contact, the water is strongly enriched with SO₄, Mg, Na, Mn, Ca, K and B, and, to a lesser degree, with Cl and Sr (Table 1). The 'marl' produces much more sulphate than the "crassin".

Table 1: Part of the water analysis results with closed reactor tests.

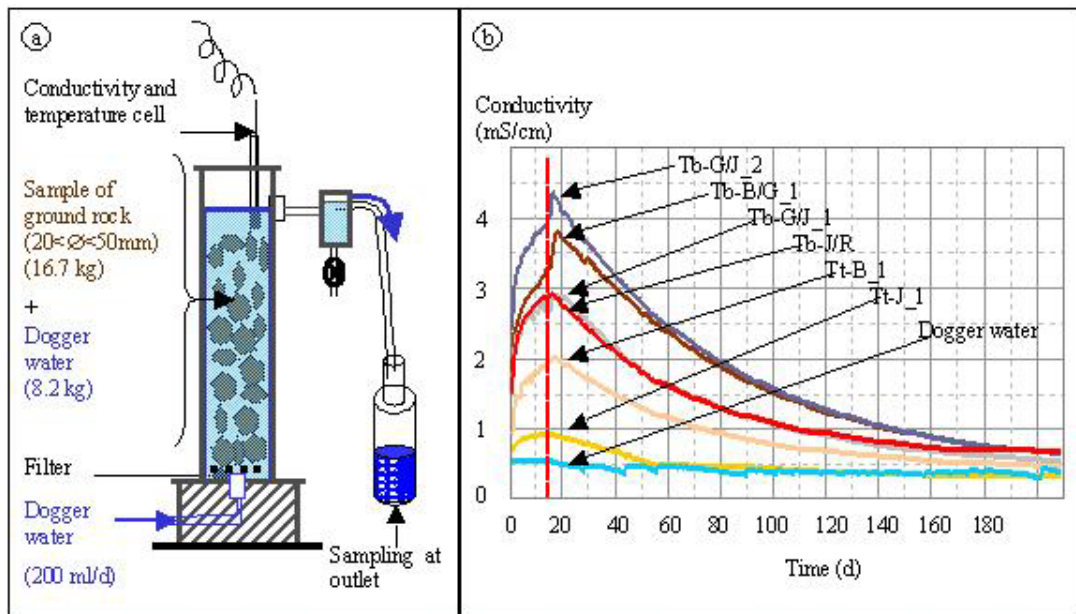
| | Cond. | pH | T° | SO ₄ | Mg | Na | Mn | Ca | K | B | Cl | Sr | Fe | HCO ₃ |
|--------------|-------|------|------|-----------------|------|------|------|------|------|-------|------|------|------|------------------|
| | mS/cm | pH | °C | mg/l | mg/l | mg/l | µg/l | mg/l | mg/l | mg/l | mg/l | mg/l | mg/l | mg/l |
| Dogger water | 0.49 | 7.57 | 26.1 | 17 | 7.8 | 3.1 | <5 | 114 | 0.7 | <0.02 | 5.3 | 0.1 | 0.04 | 283 |
| Tb-B/G_1 | 4.19 | 7.19 | 26.2 | 2963 | 357 | 376 | 8 | 518 | 13.1 | 1.53 | 31.9 | 8.7 | 0.07 | 197 |
| Tb-G/J_1 | 3.75 | 7.49 | 26.0 | 2421 | 242 | 318 | 234 | 545 | 14.1 | 1.43 | 27.2 | 9 | 0.08 | 106 |
| Tt-J_1 | 0.96 | 7.57 | 26.1 | 291 | 11.2 | 124 | 10 | 99 | 6.4 | 1.82 | 36.3 | 2.1 | 0.07 | 124 |

Cond: conductivity; Tb-B/G_1: Sample No. 1 of cross-cut between brown and grey layers; Tb-G/J_1: Sample No. 1 of cross-cut between grey and yellow layers; Tt-J_1: Sample No. 1 from top of yellow layer

Column leaching tests

Column leaching tests were performed on the same samples. Each of the six columns of the leaching system was filled with 16.3 kg of ground rock and 8 kg of Dogger water, giving the same water-rock weight ratio as in the closed reactor test (Figure 3a). The grain size distribution was identical in each column (20 mm<Ø<50 mm). In the first step, the system remained closed to approach water-rock chemical equilibrium. This phase lasted 15 days in order to compare the results of these experiments with those previously obtained on the rocks of the southern basin (Hervé, 1980). In a second step, the system was opened to observe the chemical changes in leaching conditions. Each column was supplied at its base with a flow of 200 ml/day of Dogger water. The water overflowed through an opening at the top of the column where it was regularly sampled for chemical analyses. Water conductivity and temperature in the column were measured continuously (Figure 3b).

Continuous monitoring of conductivity is an excellent indicator of SO₄, Mg, Na and Mn concentrations in water. The mineralisation observed at the start of the experiment decreased gradually until, after 180 days of leaching, identical chemical concentrations were obtained at the inlet (Dogger water) and outlet of the columns.



Designation of samples: i) Tt: top (hanging wall) or Tb: cross-cut ('-marls'). ii) Lithology: B (brown), G (grey), J (yellow), R (red), 'f' meaning 'between the layers', and iii) sample No. (up to 3 in the same layer).

Figure 3 : Principle of column leaching experiments (a) and conductivity monitoring (b)

INITIAL MINERALOGICAL COMPOSITION OF THE ROCK SAMPLES

Calculation of the state of chemical equilibrium of the water

Chemical equilibrium between the water and ore is defined by a saturation index SI: $SI = \log(IAP) - \log K(T)$ where IAP is the Ionic Activity Product and K(T) the thermodynamic equilibrium constant of this reaction. When SI = 0, the water is at equilibrium with the reagent (mineral in our case). When SI < 0 or SI > 0, the water is under- or over-saturated respectively and capable of dissolving or precipitating the mineral.

On completion of the closed reactor tests (Table 2), the saturation indexes were calculated for each solution using the PHREEQC software (Parkhurst and Appelo. 1999). Initially, the Dogger water appeared to be in equilibrium with the calcite and quartz. When water-rock chemical equilibrium was reached, on completion of the closed reactor tests, water appeared to be in equilibrium with the gypsum, calcite, quartz and different carbonates such as magnesite (MgCO₃) and strontianite (SrCO₃). These changes in the state of equilibrium provide information about the nature of the mineral phases with which the water reacts when it leaches the rock.

Table 2: Calculation of saturation indexes (Lnl database).

| | Calc | Dol | Fe | Goet | Gyp | Hém | Mag | Pyr | Qtz | Sid | Str |
|--------------|------|------|------|------|-------|-------|-------|-------|-------|-------|-------|
| Dogger water | 0.62 | 1.48 | 0.24 | 5.33 | -2.21 | 11.66 | -0.76 | <-200 | 0.05 | -10.5 | -0.53 |
| Tb-B/G_1 | 0.28 | 1.72 | 0.45 | 5.54 | -0.03 | 12.07 | -0.18 | <-200 | 0.08 | -9.79 | 0.26 |
| Tb-G/J_1 | 0.38 | 1.73 | 0.53 | 5.62 | -0.04 | 12.24 | -0.27 | <-200 | -0.05 | -10.5 | 0.36 |
| Tt-J_1 | 0.11 | 0.64 | 0.48 | 5.58 | -1.14 | 12.14 | -1.09 | <-200 | 0.2 | -10.6 | 0.23 |

Calc: calcite; Dol: dolomite; Fe: iron (III) Hydroxide; Goet: goethite; Gyp: gypsum; Hém: hematite; Mag: magnesite; Pyr: pyrite; Qtz: quartz; Sid: siderite; Str: strontianite;

Tb-B/G_1: cross-cut between brown and grey layers; Tb-G/J_1: cross-cut between grey and yellow layers; Tt-J_1: top of yellow layer.

Mineralogical origin of the different elements in solution

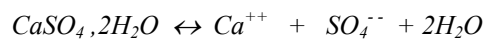
Thin sections were observed under the microscope with transmitted light and polished sections with reflected light. The samples were also analysed by X-ray diffraction. These analyses identified two types of sample 1) ‘crassin’ in the hanging wall of the mineralised layers, rich in carbonate, quartz and goethite, and 2) ‘marl’ intercalations, rich in carbonate, quartz and, to a lesser degree, goethite, but also rich in phyllosilicates. They contain a non-negligible quantity of pyrite in the form of framboidal clusters, its most reactive form (Younger *et al.*, 1998).

A quantitative chemical analysis was performed for each element in the rock. By cross-checking the results with those of the mineralogical analysis, we reconstructed a probable and coherent mineralogical composition of each sample.

MODEL OF CHEMICAL REACTIONS BETWEEN WATER AND MINERALS

Initially, using the PHREEQC software, we calculated the chemical composition of the water in thermodynamic equilibrium with the minerals defined above. The calculated water composition was then compared with the chemical analyses. The Ca, Na, K and SO₄ concentrations were closely reproduced, while those of Mg and HCO₃ deviated by one to two orders of magnitude. The new mineralogical assemblage calculated at equilibrium was not representative of the experimental results: it presumed the precipitation of albite, K-feldspar and quartz and the complete disappearance of pyrite and goethite, which are nonetheless thermodynamically very stable under the experimental conditions.

The temperature and pressure prevailing in the mine, and in the experiments, are low, reinforcing the kinetic control of the chemical reactions. To reflect these experimental results, it was necessary to construct a kinetic model of the ore dissolution and precipitation reactions in water. The formulation of the kinetics used is conventional, taking for example the gypsum dissolution and precipitation reaction:



with an equilibrium constant $K_{eq} = (Ca^{++}) (SO_4^{--}) (H_2O)^2 (CaSO_4 \cdot 2H_2O)^{-1}$ where (X) is the activity of species X .

Initially, we assumed standard conditions of temperature and pressure (25°C, 1 bar), as adopted for our laboratory experiments. The values of K_{eq} for each of the reactions were taken directly from the PHREEQC database (Parkhurst and Appelo 1999). At this stage of development of the model, the activity of the minerals and the water was considered as 1, whereas that of the gaseous species was assumed to be equal to their partial pressure. The activity of the ions is defined by: $(X) = \gamma_X [X]$, where $[X]$ is the concentration of species X in solution and γ_X its activity coefficient. The latter is taken from the equilibrium calculation performed with PHREEQC, where it is defined by the extended Debye-Hückel equation.

The total reaction rate is defined by the difference between the dissolution rate (v_d) and the precipitation rate (v_p). In the case of the above reaction, it is written: $V_t = V_d - V_p$

With $V_d = (CtI) * k_{diss}$

$$V_p = (CtI) * k_p a(Ca^{++})a(SO_4^{--})$$

The factor (CtI) enables us to introduce the concept of specific surface area into the model:

$$\langle CtI \rangle = \frac{6 M_R}{Gr \rho_R} \times \frac{m(t)}{m(0)}$$

where M_R is the total mass of rock in kg
 Gr is the mean grain size of the rock in m
 ρ_R is the mean density of the rock in kg/m³
 $m(t)$ is the mass fraction of mineral considered at t in mol/kg of rock
 $m(0)$ is the initial mass fraction of mineral in mol/kg of rock

Thus, initially, the finer the grain size distribution, the faster the reaction rate. During the reaction, the lower the quantity of mineral available, the slower the reaction rate. The dissolution constant k_{diss} and precipitation constant k_p

are apparent, because they include all the elementary mechanisms. At equilibrium, the total rate is zero so that $K_{eq} = k_{diss} / k_p$.

Based on this kinetic model, we constructed a numerical simulator using the Simulink/Matlab® software. The constants were determined from the experimental results, by fitting the model with the results of the closed reactor test performed on sample Tb-G/J_2. In this step, the chemical model contains eighteen mineral phases, all of which are taken into account in the 'calculated' composition of the rocks. Moreover, new mineral phases, known for their ability to precipitate from the dissolved elements of our system, are also introduced.

The final chemical model is defined as follows (all the parameters relate to 1 litre of solution):

| Mineral | Chemical Composition | Reaction | Log K_{eq} $T=25^{\circ}C$ | m(0) en(mol) [Tb-G/J 2] | Log k_p |
|--------------------------|----------------------------|--|---------------------------------|----------------------------|----------------------|
| Albite | $NaAlSi_3O_8$ | Albite + 4 H^+ + 8 H_2O = Na^+ + Al^{3+} + 3 H_4SiO_4 | 4.698 | $1.7146 \cdot 10^{-2}$ | $4 \cdot 10^{+5}$ |
| Chalcedony | SiO_2 | Chalcedony + 2 H_2O = H_4SiO_4 | -3.550 | $1 \cdot 10^{-9}$ | $5 \cdot 10^{-7}$ |
| Calcite | $CaCO_3$ | Calcite + H^+ = Ca^{2+} + HCO_3^- | 1.849 | 4.1609 | $8 \cdot 10^{-2}$ |
| Chlorite | $Mg_5Al_2Si_3O_{10}(OH)_8$ | Chlorite + 16 H^+ = 5 Mg^{2+} + 2 Al^{3+} + 3 H_4SiO_4 + 6 H_2O | 68.38 | $2.0459 \cdot 10^{-1}$ | $1 \cdot 10^{-10}$ |
| Dolomite | $CaMg(CO_3)_2$ | Dolomite + 2 H^+ = Ca^{2+} + HCO_3^- + Mg^{2+} | 3.658 | $8.5246 \cdot 10^{-2}$ | $5.5 \cdot 10^{-1}$ |
| Fe(OH) ₃ (am) | $Fe(OH)_3$ | Fe(OH) ₃ + 3 H^+ = Fe^{3+} + 3 H_2O | 4.891 | $1 \cdot 10^{-9}$ | $3 \cdot 10^{-5}$ |
| Gibbsite | $Al(OH)_3$ | Gibbsite + 3 H^+ = Al^{3+} + 3 H_2O | 8.110 | $1 \cdot 10^{-9}$ | $6 \cdot 10^{-6}$ |
| Goethite | $FeOOH$ | Goethite + 3 H^+ = Fe^{3+} + 2 H_2O | -1.000 | 3.9816 | $1 \cdot 10^{-10}$ |
| Gypsum | $CaSO_4 \cdot 2H_2O$ | Gypsum = Ca^{2+} + SO_4^{2-} + 2 H_2O | -4.360 | $3.5330 \cdot 10^{-2}$ | $1 \cdot 10^{-2}$ |
| Hematite | Fe_2O_3 | Hematite + 6 H^+ = 2 Fe^{3+} + 3 H_2O | -4.008 | $1 \cdot 10^{-9}$ | $5 \cdot 10^{-8}$ |
| K-Feldspar | $KAlSi_3O_8$ | K-Feldspar + 4 H^+ + 4 H_2O = K^+ + Al^{3+} + 3 H_4SiO_4 | 2.127 | $9.7251 \cdot 10^{-2}$ | $1 \cdot 10^{+6}$ |
| K-Mica | $KAl_3Si_3O_{10}(OH)_2$ | K-Mica + 10 H^+ = K^+ + 3 Al^{3+} + 3 H_4SiO_4 | 12.703 | $7.1318 \cdot 10^{-1}$ | $1 \cdot 10^{-4}$ |
| Pyrite | FeS_2 | Pyrite + 3.75 O_2 + 0.5 H_2O = H^+ + Fe^{3+} + 2 SO_4^{2-} | 224.001 | $1.6585 \cdot 10^{-1}$ | $1 \cdot 10^{-234}$ |
| Quartz | SiO_2 | Quartz + 2 H_2O = H_4SiO_4 | -3.980 | 7.7006 | $1 \cdot 10^{-9.92}$ |
| Siderite | $FeCO_3$ | Siderite + 2 H^+ + 0.25 O_2 = 0.5 H_2O^+ + Fe^{3+} + HCO_3^- | 7.939 | $2.1899 \cdot 10^{-1}$ | $4 \cdot 10^{-2}$ |
| Strontianite | $SrCO_3$ | Strontianite + H^+ = Sr^{2+} + HCO_3^- | 1.058 | $7.5819 \cdot 10^{-3}$ | $1 \cdot 10^{-7}$ |
| Other phases | | | | | |
| CO ₂ (g) | - | CO ₂ (g) + H_2O = H^+ + HCO_3^- | -7.820 | $3.33 \cdot 10^{-4}$ | 4 |
| O ₂ (g) | - | O ₂ (g) = O_2 | -2.960 | 0.21 | 1 |
| H ₂ O | - | H ₂ O = H^+ + OH^- | 14.000 | pH = 7.38 | $1 \cdot 10^{+14}$ |

The concentrations calculated after 47 days correspond relatively well to those measured in the closed reactor tests (Table 3), both for the major elements SO_4 , Ca, Mg, Na, and HCO_3^- , and for the minor elements such as Sr or K.

Table 3: Comparison of measured and calculated concentrations on the 47th day (sample Tb-G/J 2)

| | SO_4 | Ca | Mg | Na | HCO_3^- | Sr | K | pH |
|-----------------------------------|----------------------|----------------------|----------------------|----------------------|----------------------|----------------------|----------------------|------|
| Measured concentrations (mol/l) | $2.86 \cdot 10^{-2}$ | $1.45 \cdot 10^{-2}$ | $1.37 \cdot 10^{-2}$ | $1.69 \cdot 10^{-2}$ | $1.05 \cdot 10^{-3}$ | $1.05 \cdot 10^{-4}$ | $4.3 \cdot 10^{-4}$ | 7.67 |
| Calculated concentrations (mol/l) | $2.63 \cdot 10^{-2}$ | $9.86 \cdot 10^{-3}$ | $8.81 \cdot 10^{-3}$ | $1.67 \cdot 10^{-2}$ | $7.5 \cdot 10^{-4}$ | $1.01 \cdot 10^{-4}$ | $1.05 \cdot 10^{-4}$ | 7.38 |

The consistency of the results obtained with this model enables us to suggest several hypotheses concerning the chemical reactions causing mineralisation of the water during flooding of the Lorraine iron mines.

The high sulphate concentrations results from the dissolution of gypsum. The gypsum is produced during cutting of the mine galleries, through the oxidation of pyrite and neutralisation by carbonates. The detrital weathering of the albite is responsible for the high sodium concentrations in the overflow discharge, confirming the hypotheses already formulated in 1992 during a petrographic and structural analysis. Magnesium would result chiefly from the dissolution of chlorite and potassium from the dissolution of K-Feldspar. However, the iron concentrations are poorly reproduced. This could be explained by the detection limit of the analytical method employed to determine this element in water

(measured values equal to the detection threshold). The variation in chlorine content during leaching of the rocks is about $6 \cdot 10^{-4}$ mol/l and could be due to the leaching of chloride ions present in the intermediate layers of chlorite. This reaction was not modelled.

The chemical model offers a better understanding of the mechanisms controlling the mineralisation of the water during flooding of the Lorraine iron mines.

CONCLUSION

The Lorraine iron basin falls into the as yet little-investigated context of neutral mine drainage due to the presence of carbonates. Experiments in closed reactors and column leaching tests performed on different rocks of the Lorraine iron basin have enabled us to clarify changes in water chemistry during flooding. The water is strongly mineralised (up to 3 g/l SO₄) during contact with the marly intercalations, rich in pyrite and phyllosilicates. This results in an enrichment of SO₄, Mg, Na, Mn, Ca, K and B, and, to a lesser degree, Cl and Sr.

Based on the results of mineralogical and chemical analysis of the rocks, we reconstructed a probable mineralogical composition of each sample. These data were in turn used in chemical thermodynamic equilibrium calculations. A chemical model integrating the kinetics of the reactions was constructed and applied to the simulation of tests in closed reactors. It provided results close to the experimental observations and thereby served to give a more accurate definition of the mechanisms causing mineralisation of the water during flooding of the Lorraine iron mines. Thus the dissolution of gypsum, albite, chlorite and K-Feldspar, the combined dissolution/precipitation reactions of calcite, dolomite, siderite, and the precipitation of iron hydroxide and chalcedony, can explain the high SO₄, Na, Ca, Mg and HCO₃ concentrations observed in the overflow discharge.

The prospects of this work are now focused on coupling this chemical model with a transport model. The initial aim will be to simulate column leaching tests. This will be followed by a simulation of the mineralisation at the actual overflow point of the Lorraine iron basin.

ACKNOWLEDGMENTS

This work forms part of the research programme carried out by GISOS (*Groupement de recherche sur l'Impact et la Sécurité des Ouvrages Souterrains – Research Group for the impact and safety of artificial underground cavities*).

REFERENCES

- Bequette B.W. (1998) – *process dynamics- Modeling, Analysis, and Simulation*, Prentice hall PTR, 622 p.
- Brown P.L., Lawson R.T. (1997) - *The use of kinetic modelling as a tool in the assesment of contaminant release during rehabilitation of a uranium mine*, Journal of Contaminant Hydrology, Vol. 26, 27-34
- Bubenicek L. (1970) - *Géologie du gisement de Fer de Lorraine*, Doctoral thesis, Faculty of Science of the University of Nancy, CNRS No.: A.O. 3731
- Donovan J.J., Leavitt B., Werner E., Perry E., McCoy K. (2000) - *Long-term hydrogeological and geochemical response to flooding of an abandoned below-drainage Pittsburg coal mine*, West Virginia University, 19 p.
- Hervé D. (1980) - *Etude de l'acquisition d'une teneur en sulfate par les eaux stockées dans les mines de fer de Lorraine*, Doctoral thesis, Institut National Polytechnique de Lorraine
- Mayo A.L., Petersen E.C., Kravits C. (2000) - *Chemical evolution of coal mine drainage in a non-acid producing environment, Wasatch Plateau, Utah, USA*, Journal of Hydrology, No. 236, 1-16
- Parkhurst D.L., Appelo C.A.J. (1999) - *User Guide to PHREEQC (Version 2) - a computer program for speciation, batch-reaction, one-dimensional transport, and inverse geochemical calculations*: U.S. Geological Survey Water-Resources Investigations Report 99-4259, 312 p.
- Razowska L. (2001) - *Changes of groundwater chemistry caused by the flooding of iron mine (Czestochowa Region, Southern Poland)*, Journal of Hydrology, No. 244, 17-32
- Rose A.W., Cravotta C. A. (2001) - *Coal Mine Drainage prediction and pollution prevention in Pennsylvania, Chapter 1* The Pennsylvania Department of Environmental Protection USGS, USA
- Salomons W. (1995) - *Environmental impact of metals derived from mining activities: processes, prediction, prevention*, Journal of Geochemical Exploration, No. 52, 5-23.
- Smith M.W., Brady K.B.C. (2001) - *Coal Mine Drainage prediction and pollution prevention in Pennsylvania, Chapter 13*. The Pennsylvania Department of Environmental Protection USGS, USA
- Smith E.E., Svanks K.S. (1970) - *Sulfide to sulfate reaction mechanism*, Water pollution control research series, report
- Younger P.L., Banwart S.A., Nuttal C., Jarvis A.P. (1998) - *Mine waste and minewater pollution – Short course*, The Mining Institute, Newcastle Upon Tyne